# Hydrophobic Zeolites for Biofuel Upgrading Reactions at the Liquid−Liquid Interface in Water/Oil Emulsions

Paula A. Zapata,[#] Jimmy Faria,[#] M. Pilar Ruiz, Rolf E. Jentoft, and Daniel E. Resasco*

School of Chemical, Biological and Material Engineering, and Center for Interfacial Reaction Engineering, University of Oklahoma, Norman, Oklahoma 73019, United States

ABSTRACT: HY zeolites hydrophobized by functionalization with organo-silanes are much more stable in hot liquid water than the corresponding untreated zeolites. Silylation of the zeolite increases hydrophobicity without significantly reducing the density of acid sites. This hydrophobization with organosilanes makes the zeolites able to stabilize water/oil emulsions and catalyze reactions of importance in biofuel upgrading, i.e., alcohol dehydration and alkylation of *m*-cresol and 2-propanol in the liquid phase, at high temperatures. While at 200 °C the crystalline structure of an untreated HY zeolite collapses in a few hours in contact with a liquid medium, the functionalized hydrophobic zeolites keep their structure practically unaltered. Detailed XRD, SEM, HRTEM, and BET analyses indicate that even after reaction under severe conditions, the hydrophobic zeolites retain their crystallinity, surface area, microporosity, and acid density. It is proposed that by preferentially anchoring hydrophobic functionalities on the external surface, the direct contact of bulk liquid water and the zeolite is hindered, thus preventing the collapse of the framework during the reaction in liquid hot water.
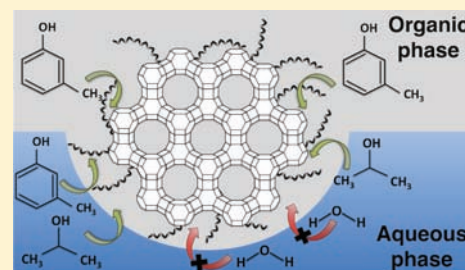
1. INTRODUCTION

Biomass has a highly oxygenated structure, which after thermochemical conversion results in liquid products of low vapor pressure, high solubility in water, and high reactivity. These characteristics impede conventional thermal upgrading processes in vapor phase,[1] and so they make liquid-phase processing attractive. In fact, aqueous solutions have been successfully used in different catalytic strategies for biomass conversion, including hydrolysis of cellulose[2] and isomerization/dehydration of monosaccharides.[3] In such cases, water is the obvious solvent of choice for its relatively low cost, minimal environmental impact, and ability to solubilize oxygenated biomass products in high concentrations. While zeolites have been intensely investigated as catalysts in the vapor-phase processing of lignocellulosic biomass, they have not been widely used in aqueous media. A major drawback of zeolites is their low tolerance to hot liquid water (i.e., >150 °C). Under this severe environment most zeolites lose their crystalline structure and consequently their catalytic activity.[4] Overcoming this limitation is a key challenge for the development of liquid-phase upgrading processes for biofuel production.

The density of Brønsted and Lewis acid sites in zeolites depends on the Si/Al ratio, the framework configuration, and the type of cation used for charge compensation.[5] Likewise, their stability in hot liquid water is also related to these properties. For instance, it has been proposed that in hot liquid water faujasite degrades via hydrolysis of Si−O−Si bonds to an amorphous material with greatly reduced catalytic activity[4,6] to a level that depends on the Si/Al ratio. Increasing the Si/Al ratio is an effective way of improving catalyst stability in aqueous environments because it increases the hydrophobic

character of the zeolite.[7] In fact, Corma et al.[8,9] have developed Al-free hydrophobic Sn-beta zeolites that can act as weak Lewis acid sites, even in the presence of condensed water. Based on these concepts, Moliner et al.[10] have recently used these (Al-free) Sn-beta zeolites to isomerize glucose to fructose in an acid aqueous environment. Unfortunately, to eliminate hydrophilicity this approach requires sacrificing the Brønsted acid sites, which inhibits the use of these catalysts for Brønsted acid-catalyzed reactions, such as dehydration, alkylation, and oligomerization. Moreover, the synthesis methods needed to make the defect-free, Al-free zeolites involve the utilization of environmentally unfriendly media, such as HF.[10]

An alternative method to increase hydrophobicity without reducing the density of acid sites is the silylation of the external surface with organosilanes.[11,12,14] We have previously shown[15−17] that hydrophobic carbon nanotubes fused to hydrophilic metal oxides are capable of simultaneously stabilizing water/oil emulsions and catalyzing reactions at the liquid−liquid interface. These amphiphilic particles have proven to be effective in the liquid-phase upgrading of bio-oil.[18] A remarkable property of these materials is their high affinity for the liquid−liquid interfaces,[19] which allows them to stabilize emulsions of small droplet size. In addition, they enhance the liquid−solid−liquid interfacial area, can facilitate the separation of molecules from the reaction system, and open the possibility of selectively converting molecules in only one of the liquid phases (i.e., phase-selectivity), simply based on differences in solubility.[18,20]

In this contribution, we report the use of surface-modified faujasites as stabilizers of water/oil emulsions and as catalysts for the alkylation of (organic-soluble) phenolics with (aqueous-soluble) alcohols. Moreover, it is demonstrated that these hydrophobic zeolites are much less susceptible to degradation in hot liquid water than conventional zeolites. This approach could have a major impact in the liquid-phase upgrading of bio-oil and polysaccharides, where biphasic reaction systems are desirable since they lead to higher product yields favored by the rapid separation of products from the aqueous phase, which prevents undesired repolymerization.[21,22]

2. EXPERIMENTAL SECTION

2.1. Materials and Methods. The zeolite used in this work was a faujasite HY zeolite, type CVB760, provided by Zeolyst International and used as received. The manufacturer of the CVB760 zeolite reports a Si/Al molar ratio of 30, a surface area of 720 m^2/g, and an unit cell of 24.24 Å. That is, this zeolite has been partially dealuminated to increase its thermal stability.

To functionalize the surface of the zeolite, we followed a previously described silylation procedure[23] that uses octadecyltrichlorosilane (OTS) as a silylating agent. Briefly, in this procedure, 1 g of the untreated HY zeolite is dispersed in 20 mL of toluene by sonication with a Horn sonicator (Fisher Scientific 600 W, 20kHz) at 25% amplitude. Then, the zeolite suspension is added to a 50 mL solution of OTS (0.5 mmol/g zeolite) in toluene (OTS and toluene provided by Sigma Aldrich). The final suspension was stirred for 24 h at 500 rpm at room temperature. The zeolite was then collected by filtration with a nylon filter (0.22 μm pore size). After washing several times with ethanol, the functionalized zeolite was dried at 100 °C overnight.

2.2. Characterization of the Zeolites. Several techniques were employed to characterize the properties and structure of both untreated and functionalized zeolites, before and after reaction in the liquid phase. They include diffuse reflectance infrared Fourier transformation spectroscopy (DRIFT), thermogravimetric/differential thermal analysis (TG-DTA), temperature-programmed oxidation (TPO), X-ray diffraction (XRD), scanning electron microscopy (SEM) and high-resolution transmission electron microscopy (HRTEM), and N_2 physisorption.

DRIFT spectra were recorded on a Perkin-Elmer Spectrum 100 FTIR, equipped with a high temperature DRIFT cell (HVC, Harrick) with CaF_2 windows. The sample powder (100 mg) was placed in the cell, heated in situ up to 250 °C under a flow of He (30 mL/min) with a ramp of 10 °C/min, and kept at this temperature for 30 min. A background spectrum was recorded in each run followed by 256 scans taken at a resolution of 4 cm^{-1} to obtain the final average spectrum. For the pyridine adsorption experiments, the samples were outgassed in He at 350 °C and then cooled in He to 100 °C; subsequently, the samples were exposed to a stream of −20 °C saturated pyridine in He. After pyridine exposure, the sample was purged in He at 100 °C for 3 h, and the DRIFT spectra were recorded.

To study the behavior of the functionalized zeolite with temperature and to quantify the amount of carbon anchored on the zeolite surface during the silylation process, we conducted TG-DTA and TPO of the OTS-functionalized zeolite. The thermogravimetric analysis was conducted using a Netzsch STA 449 F1 Jupiter TG-DTA. The sample was treated in air at 100 °C for 30 min, followed by a heating ramp of 10 °C/min to 800 °C, and a cooling ramp of 20 °C/min to 400 °C. Measurement of the variation of weight as a function of temperature was complemented with IR analysis of the evolved gases using a coupled Bruker Tensor 27 FTIR.

TPO was conducted on the functionalized zeolite passing an 80 mL/min continuous flow of 5% O_2/He. The sample (~30 mg) was located in a quartz tube reactor and the temperature was increased at 10 °C/min up to 900 °C. During this process, the exit gases were sent through a methanator consisting of a 5% Ni/Al_2O_3 catalyst with a H_2 side-stream that converts CO and CO_2 into CH_4, which can be detected by a highly sensitive flame ionization detector (FID). To quantify the amount of carbon deposited the FID signal was calibrated with a 100 μL CO_2 reference pulse.

XRD patterns were collected on a D8 Series II X-ray diffractometer (BRUKER AXS), in reflection geometry using Cu Kα radiation generated at 40 kV and 35 mA. The scans covered the 2θ range from 10° to 35°. SEM images were obtained on a JEOL JSM-880 high-resolution scanning electron microscope with a useful magnification of up to 300,000×. HRTEM images were obtained on a JEOL 2010-F, a scanning transmission research electron microscope with field emission intermediate voltage (200 kV), with magnification of up to 8,000,000×.

The BET surface areas, pore volume, and pore size distributions were obtained by N_2 physisorption in a Micromeritics ASAP 2010 unit. The mesopore size distribution was obtained using the Barrett−Joyner−Halenda (BJH) technique, while the distribution of micropores was estimated using Density Functional Theory (DFT) analysis;[24] both methods are incorporated in the Micromeritics analysis package.

2.3. Preparation of Particle-Stabilized Emulsions. To check the ability of the different zeolites to stabilize water/oil emulsions, 30 mg portions of each zeolite were added to a 10 mL mixture of deionized water and decalin (vol. ratio 1:1). Emulsions were prepared by sonicating for 30 min with an ultrasonic horn operating at 25% of max. amplitude. After sonication, the suspension was left to settle for 24 h before measuring the resulting fraction of emulsion formed and droplet size (by optical microscopy).

2.4. Reaction System. Catalytic rate measurements (alcohol dehydration and m-cresol/2-propanol alkylation) were carried out in a 300 mL Parr 4843 reactor. The temperature inside the reactor was controlled with a CAL 9500P controller (CAL Controls Ltd.). An Aschcroft pressure transducer was used to monitor the pressure inside the reactor. In each run, a 0.5 g catalyst sample was dispersed in a 60 mL mixture of equal volumes of deionized water and decalin, ultrasonicating as described above. The mixture was placed in the stainless steel reaction vessel and purged with a 200 mL/min flow of He. The pressure was increased to 300 psi, while stirring at 80 rpm, and the reactor was heated up to 200 °C. At this point, 25 mL of a mixture of equal volumes of deionized water and decalin containing the reactants was injected from a pressurized feeding cylinder. The pressure of the reactor was adjusted to 700 psi with additional He and finally the gas inlet was closed to let the reaction proceed in the batch mode. At the end of the reaction period, the reactor was cooled to room temperature and depressurized. To break the emulsion before analysis the nanohybrid particles were filtered out in two steps. First, coarse paper filter (8 μm pore) trapped a large fraction of the solid particles, which quickly agglomerate over the surface of the filter. In the second step, a PTFE (0.2 μm pores) filter was used to separate the remaining catalyst particles that passed the first filter. The two clear liquid phases obtained after filtration were separated and samples of each phase were analyzed by gas chromatography (GC-FID and GC-MS). An Agilent GC-FID 6890A equipped with a capillary column of polyethylene glycol (HP-INNOWAX) of 60.0 m × 0.32 mm × 0.25 μm nominal was used for quantitative analysis, while a Shimadzu QP2010S GC-MS equipped with an HP-INNOWAX polyethylene glycol capillary column, 30.0 m long × 0.25 μm nominal, was used for product identification, by using standards for those compounds that are commercially available. In all the GC-FID analyses, ethanol and 1,2-dichloromethane were used as internal standards to help close the mass balances. To minimize column damage, the aqueous fractions were extracted in methanol before injection.

3. RESULTS AND DISCUSSION

3.1. Characterization of the Zeolites before Reaction. The combination of techniques employed to characterize the functionalized zeolites provides a complete picture of their structure and composition. Figure 1 shows the DRIFT spectrum for HY zeolite (a), OTS-functionalized HY zeolite (b), the functionalized zeolite after high-temperature solvent treatment, at 200 °C for 3 h (bs), and after calcining in air at
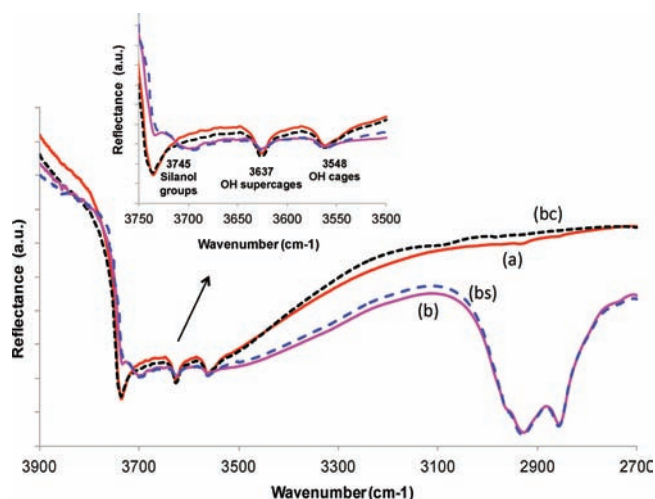
Figure 1. DRIFT spectra of (a) untreated HY zeolite; (b) OTS-functionalized HY zeolite; (bs) functionalized zeolite after 3 h treatment in biphasic solvent (water/decalin) at 200 °C; and (bc) functionalized zeolite after calcination in air at 450 °C for 16 h. Inset: OH region expanded.

450 °C for 16 h (bc). An important characteristic exhibited by the hydrophobic zeolite is the presence of intense bands in the 2800−3000 cm^{-1} region. These bands are absent in both the untreated and the functionalized zeolite heated to high temperature. Since they are in the region of C−H bond stretching, they can be attributed to the C−H bonds of the OTS attached to the zeolite.[25] Specifically, the stretching vibrations corresponding to the observed bands are grouped in three types, symmetric methylene (−CH$_2$), antisymmetric methylene (−CH$_2$), and methyl (−CH$_3$), appearing centered around 2855, 2925, and 2965 cm^{-1}, respectively,[26−28] in good agreement with the bands observed here on the functionalized zeolite. Small shifts and band broadening have been observed as a result of variations in surface concentration of OTS,[29] which may explain the observed widths of the bands.

Another important difference between the zeolites is seen for the bands associated with the single and geminal silanol groups.[30] While on the untreated hydrophilic zeolite an intense and rather narrow band appears at 3745 cm^{-1}, on the hydrophobic one the band is much weaker and appears shifted to lower frequency (3700 cm^{-1}) due to the interaction with OTS molecules. Moreover, after heating in air (450 °C), the intense band at 3745 cm^{-1} reappears and the spectrum looks essentially the same as that of the untreated zeolite.

An even more important observation of significant relevance to the activity data shown below is that, both functionalized and untreated samples exhibited the characteristic bands of high-frequency (HF) and low-frequency (LF) hydroxyl vibrations (3637 and 3548 cm^{-1}, respectively). These bands are typically associated with Brønsted acid sites,[31−34] responsible for the activity for the reactions investigated in this work. In HY zeolites, the HF bands are attributed to hydroxyl groups of the supercages while the LF bands are associated with those inside the small β-cages.[31,35] It is worth noting that while the intensity of these bands seems weaker after functionalization, they appear at the same frequencies for both untreated and functionalized zeolites, which can be taken as an indication of a low extent of OTS attachment to any of the internal sites (small cages or supercages) and preferential anchoring onto the external surface.

We have quantified the amount of OTS functional groups anchored to the zeolite surface during the silylation process by TG-DTA and TPO analyses. The TG-DTA results are shown in Figure 2. A total weight loss of 13.8% was observed in several
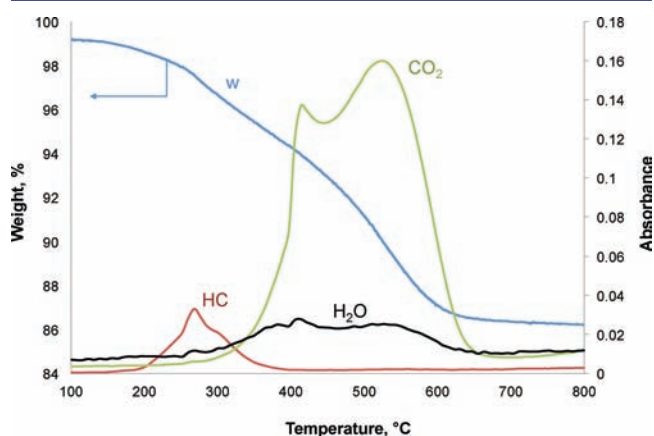

Figure 2. Thermogravimetric analysis (TG-DTA) of the untreated and OTS-functionalized HY zeolite (Si/Al = 30). Left axis: Weight (%). Right axis: IR absorbance due to water (3735 cm^{-1}), hydrocarbon C−H stretching (2962 cm^{-1}), and CO$_2$ (2350 cm^{-1}).

stages. First, a loss of 0.8% was observed during the isothermal 40 min period at 100 °C. A second weight loss of 3.4% was obtained at the beginning of the heating ramp from 100 to about 350 °C (max. 250 °C), and a final more pronounced loss of about 9.6% was seen in the range 350−600 °C (max. 390, and 500 °C). These losses are attributed to a combination of water desorption and OTS decomposition. IR spectra of the gas phase obtained during the temperature ramp mainly exhibit bands for H$_2$O (numerous peaks centered at 1600 and 3790 cm^{-1}), CO$_2$ (2280−2390 cm^{-1}), CO (2100 cm^{-1}) and hydrocarbons (2800−3000 cm^{-1}). Figure 2 illustrates the intensity variation of three specific bands: (i) 3735 cm^{-1} (due to water), (ii) 2962 cm^{-1} (due to C−H stretching vibration in hydrocarbons); and (iii) 2350 cm^{-1} (due to CO$_2$). From the combined variation of weight and IR analysis it can be concluded that the initial 1% loss during the isothermal period at 100 °C is mostly due to water desorption. An additional 3 wt % is lost between about 200 and 340 °C. In this range, there is only a small increase in intensity of bands consistent with the desorption of hydrocarbons. However, between 350 and 650 °C, the weight loss is 9.6% with a simultaneous increase in the intensity of the H$_2$O and CO$_2$ bands, consistent with the combustion of the hydrocarbon functionalization. The steeper changes in weight loss, correspond very well with the peaks of H$_2$O and CO$_2$ evolution at 400 and 550 °C.

To better differentiate and quantify the water loss and OTS decomposition, we conducted TPO on the hydrophobized zeolite. TPO only measures carbon evolution by converting it to CO and CO$_2$. This measurement yielded an amount of carbon of about 5.7 wt%, which corresponds to a mass of OTS of 6.7 wt%. This means that of the total 13.8% weight loss observed in the TG-DTA analysis about 7.1% could be attributed to water. As expected, this is somewhat lower than the amount of water losses typically measured when heating an untreated zeolite, i.e., approximately 10%.[36,37]

From this analysis and the known external surface area of the CBV760 zeolite,[38] we can estimate that the amount of carbon associated with the OTS functional groups, i.e., 260 μmol of

OTS per gram of zeolite would correspond to a surface density of about 1−2 functional groups per nm^2, which is the typical surface density of silanol groups on the external surface of this zeolite.[39] This is another indication that the functionalization occurs preferentially at the external surface.

The TGA studies suggest that, under the conditions used for the alcohol dehydration and alkylation reactions (200 °C and in absence of oxygen), the integrity of the OTS functional groups should be preserved. However, to further support this conclusion we conducted an additional experiment. The functionalized zeolite was placed in the reactor in contact with a mixture of water and decalin, the two solvents used in the reaction experiments, and heated to 200 °C for 3 h in 700 psi He. After this period, the sample was recovered by filtration, dried at 100 °C, and analyzed by FTIR to confirm that the intensity of the bands due to OTS do not decrease, nor do the bands due to sylanol OH increase. As compared in Figure 1, this is indeed the case. There was practically no change in the entire spectrum of the functionalized zeolite after heating in the biphasic solvent.

Another important consideration is whether the functionalization occurs preferentially on the external surface of the zeolite, leaving the Brønsted and Lewis acid sites largely unaltered, or to the contrary, whether the functionalization causes a significant loss in acid density. To answer this question, we have conducted FTIR analysis of adsorbed pyridine on both the untreated and the OTS-functionalized HY zeolites. The corresponding DRIFT spectra on the two zeolites before and after exposure to pyridine at atmospheric pressure and 100 °C are presented in Figure 3. Upon chemisorption on acidic
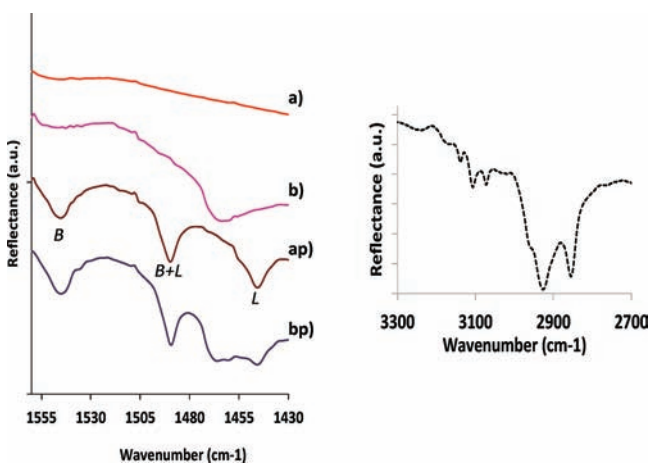

Figure 3. DRIFT spectra of the pyridine chemisorption experiments at 100 °C and atmospheric pressure for the different HY zeolites (Si/Al = 30): (a) untreated HY zeolite, (b) OTS-functionalized HY zeolite, (bp) functionalized HY zeolite after pyridine chemisorption, (ap) untreated HY zeolite after pyridine chemisorption. Right: DRIFT spectra of the region around 2900 cm^{-1} of the functionalized HY zeolite after pyridine chemisorption.

zeolites, pyridine exhibits characteristic IR absorption bands at 1545 cm^{-1} when adsorbed on Brønsted acid sites (i.e., forming a pyridinium ion), and at 1450 cm^{-1} when adsorbed in Lewis sites.[40,41] As shown in the spectra, both bands are clearly present on the two zeolites, with very similar intensities, which clearly shows that most of the original Brønsted and Lewis acid sites remain unaffected after the OTS functionalization. Also, as shown in Figure 3, the characteristic C−H bands of the

functionalization (see Figure 1) are present and largely unaffected during the pyridine adsorption experiments. It is not clear why while the density of acid sites is essentially unchanged, the intensity of the HF and LF hydroxyl bands appears somewhat weaker for the functionalized zeolite. However, as shown below, functionalization does not cause any loss in the catalytic activity of these acid sites, which is the most important outcome.

3.2. Particle-Stabilized Emulsions. An obvious difference in the behavior of hydrophobic zeolites with respect to the conventional hydrophilic is observed when they are immersed in a mixture of deionized water and decalin (Figure 4a). While
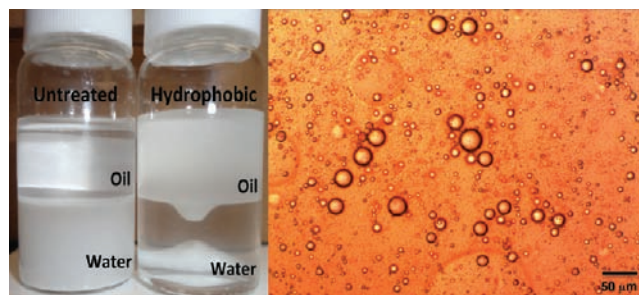

Figure 4. Left: Distribution of the untreated and OTS-functionalized HY zeolite in a biphasic water/decalin system. Right: Optical microscopy image of the water/decalin emulsion stabilized by functionalized HY zeolite (Si/Al = 30).
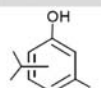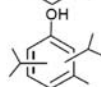
the untreated zeolites rapidly settle to the bottom of the aqueous phase, the OTS-functionalized zeolite disperses in the oil phase and stabilizes the water−decalin interface. Moreover, when the functionalized zeolite mixture is sonicated, a stable emulsion of very small water droplets (∼5 μm) dispersed in the organic phase is obtained (Figure 4b). The calculated liquid−liquid interfacial area of this emulsion is approximately 10 m^2/g zeolite. By contrast, the untreated zeolite does not produce a stable emulsion.

3.3. Catalytic Activity in the Emulsion. To compare the activity of the untreated and functionalized zeolites in aqueous environment at high temperatures, we studied the alkylation of m-cresol with 2-propanol in a water/decalin emulsion. Alkylation of m-cresol is an industrially important reaction that produces the precursors for a number of commercially valuable chemicals.[42] Moreover, in reference to biofuel production, alkylation of phenolics with alcohols is an attractive strategy to retain carbon in the liquid products of biomass pyrolysis. Bio-oils contain significant amounts of C$_1$−C$_3$ acids, which can be ketonized and then hydrogenated to short alcohols. For example, acetic acid is a major component of bio-oil, and it can be ketonized to acetone, which is readily hydrogenated to 2-propanol. These alcohols can act as alkylating agents of the phenolic fraction of bio-oil and be incorporated in the final liquid product instead of being lost as light gases during a final hydrotreating refining step. Among the alkylated products from the reaction of m-cresol and 2-propanol, 2-isopropyl-5-methylphenol (thymol) is an important precursor of menthol, a compound highly used in the pharmaceutical industry and perfumery.[43]

In this study, we used 2-propanol and m-cresol as a feed (molar ratio 3:1), keeping a total concentration of 2 M in single aqueous phase or in a water/decalin biphasic system. Thymol from Sigma Aldrich was used as standard for the GC

calibration. Table 1 summarizes the results of the alkylation reaction at 200 °C and 700 psi of He on both untreated and

Table 1. Alkylation of *m*-Cresol with 2-Propanol in Single (Aqueous) Phase and Biphasic (Emulsion) Systems[a]

| zeolite | single aqueous phase | | | | emulsion (water/decalin) | | | |
| | untreated | | functionalized | | untreated | | functionalized | |
	1.33 h	3 h	1.33 h	3.h	1.33 h	3 h	1.33 h	3 h
(OH structure)	1.8	2.3	2.22	7.3	2.6	6.6	6.9	13.0
(OH structure)	0.2	1.1	0.6	3.0	1.0	2.5	3.0	6.5
m-cresol conversion (%)	2.0	3.3	2.8	10.3	3.6	9.1	9.9	19.5

[a]Comparison of overall conversion and product distribution at 200 °C and 700 psi of He over untreated and OTS-functionalized HY zeolite (Si/Al = 30) at two reaction times. The feed had a total concentration of 2 M, with a 2-propanol/*m*-cresol molar ratio of 3:1.

OTS-functionalized zeolite in the single and two-phase systems. It can be noted that with both untreated and functionalized zeolite, the *m*-cresol conversion was higher in the biphasic system than in the single aqueous phase.

As an example, after 3 h of reaction with the functionalized zeolite as catalyst, the *m*-cresol conversion was ~10% in single aqueous phase, and ~20% in biphasic (emulsion) system with corresponding increase in yields of mono and dialkylated products, which proves the higher efficacy of the emulsion system, probably due to the increase in the interfacial area.[16−20] Moreover, the hydrophobic OTS-functionalized zeolite exhibited a much higher activity than the untreated zeolites. For example, in the 3 h reaction in the biphasic system, the conversion of *m*-cresol was only 9.1% with the untreated zeolite, but 19.5% for the functionalized zeolite. One can expect that the diffusion of water molecules to the interior of the hydrophobic zeolite will be hindered by the presence of the functional groups. By contrast, while 2-propanol mostly resides in the aqueous phase, its transport through the organic functional groups will be less restricted than that of water, a molecular discrimination that does not occur on the untreated zeolite.

To test this concept, we conducted the dehydration of 3-pentanol to pentene and 2-propanol to propylene in a biphasic (1:1) water/decalin system at 200 °C and 700 psi of He. As shown in Table 2, a significant difference in dehydration activity was observed after 3 h reaction between the two zeolites. While the untreated zeolite reached conversions of 26−27%, the functionalized zeolite reached 85−88%. That is, inside the

Table 2. Alcohol Conversion in the Dehydration Reactions of 3-Pentanol or 2-Propanol at 200 °C and 700 psi of He over Both Untreated and OTS-Functionalized HY Zeolites (Si/Al = 30)[a]

| conversion (%) | zeolite | |
	untreated	functionalized
3-pentanol to pentene	27.3	85.0
2-propanol to propylene	25.9	88.1

[a]Feed: 3-pentanol or 2-propanol with a total molar concentration of 1 M. Reaction: 3 h in biphasic (emulsion) system.

zeolite, the alcohols are rapidly dehydrated to the corresponding olefins, which can easily form the carbenium ion alkylating agent. *m*-Cresol partitions between the two phases, and it can access the zeolite from either phase. We have compared the uptake rates of 2-propanol and *m*-cresol from aqueous and organic solutions into the functionalized and untreated zeolites, directly measured in suspension at room temperature. Table 3

Table 3. Adsorption Rates [mmol (g of zeo)$^{-1}$ h^{-1}] of *m*-Cresol and 2-Propanol from Aqueous or Organic (Decalin) Solution on OTS-Functionalized HY and Untreated HY Zeolites (Si/Al = 30)[a]

| | aqueous phase | | organic phase | |
	functionalized	untreated	functionalized	untreated
2-propanol (2POL)	2.0	2.4	10	8.5
m-cresol (MCR)	10.8	3.0	11	4

[a]Uptake measurements as a function of time were conducted in a batch-stirred glass system at room temperature and atmospheric pressure.

summarizes the adsorption rate measurements. In general, the highest adsorption rates for both adsorbates were observed from the oil phase. However, it is remarkable that the adsorption of cresol on the hydrophobic functionalized zeolite is very high even from the aqueous phase.

Even though the kinetics of a surface reaction is governed by chemical potentials rather than concentrations, and solubility is not a crucial parameter for surface kinetics,[44] the rate of mass transport is directly affected by solubility. In this case, the hydrophilicity or hydrophobicity of the zeolite seems to play a crucial role in determining the rate of reactions occurring inside the pores.

Figure 5 shows the time evolution of conversion and concentration of alkylated products during the reaction of *m*-cresol and 2-propanol in the emulsion systems at 200 °C and 700 psi of He over the functionalized zeolite. It is observed that the conversion of *m*-cresol increases with time up to about 75% after 18 h reaction. The growth in concentration of the dialkylated product starts with zero slope, then increases and
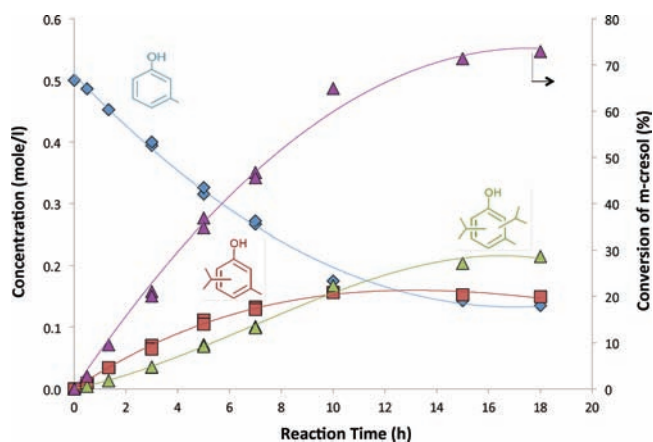

Figure 5. Alkylation of *m*-cresol with 2-propanol in the biphasic (emulsion) system at 200 °C and 700 psi of He over OTS-functionalized HY zeolite (Si/Al = 30) as a function of reaction time. Left axis: Product distribution. Right axis: Overall *m*-cresol conversion. The feed had a total concentration of 2 M with a 2-propanol/*m*-cresol molar ratio of 3:1.

reaches a plateau. By contrast, the concentration of the monokylated product reaches a maximum at about 10 h, and then decreases slightly as a result of further alkylation.

Figure 6 compares the time evolution of conversion for the two zeolites. A clear difference is observed between the
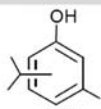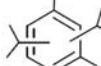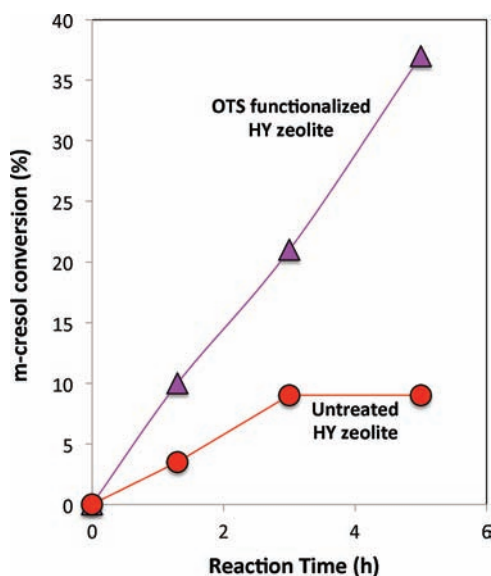

Figure 6. Conversion of *m*-cresol as a function of reaction time during alkylation with 2-propanol at 200 °C and 700 psi in He over two HY zeolites (untreated and OTS-functionalized). Alkylation reaction conditions are the same as those in Figure 5 and Table 1.

hydrophobic and hydrophilic zeolites. While the former (OTS-functionalized) shows a continuous increase in the *m*-cresol conversion with reaction time, the latter (untreated) seems to lose its activity quite rapidly. For instance, while conversion on the hydrophobic zeolite from 3 to 5 h of reaction goes from 21 to 37%, no change in conversion is observed with the untreated zeolite after 3 h. That is, the hydrophilic catalyst is completely deactivated at this point.

3.4. Catalyst Regenerability and Reusability. To further compared the stability of these catalysts during reaction and evaluate their potential regenerability and reusability the following experiments were conducted. First, the alkylation of *m*-cresol with 2-propanol was run for 3 h in the batch reactor as described above. After this first reaction period, the resulting liquid was separated from the catalyst by centrifugation at 5000 rpm for 5 min. The solid was washed first with water, then with decalin, and finally centrifuged again to separate it from the liquid. The resulting solids were dried overnight in an oven at 100 °C. To preserve the hydrophobicity of the OTS zeolite, no other high-temperature regeneration method was employed. Since a significant fraction of catalyst is lost during the separation, washing, and drying process, in order to compare the activity of the used (and dried) catalysts with the original catalyst, the catalysts of two runs were combined in order to load the same amount of catalyst in the reactor for the second reaction run. The comparison of activity between the first run and the second run with the two zeolites is made in Table 4. A remarkable difference is observed. While the OTS-function-alized zeolite is seen to retain a large fraction of its original activity (~85%) after regeneration and reuse, the untreated zeolite has completely lost its activity.

Table 4. Reusability of the Untreated and OTS-Functionalized HY Zeolites[a]

zeolite	functionalized		untreated	
	first run	second run	first run	second run
(OH, isopropyl-substituted cresol structure)	13.0(+/-0.5)	10.9(+/-0.3)	5.8(+/-0.2)	<0.01
(OH, isopropyl-substituted cresol structure)	6.4(+/-0.2)	5.3(+/-0.3)	2.5(+/-0.1)	<0.01
m-cresol conversion (%)	19.5(+/-0.4)	16.2(+/-0.6)	9.1(+/-0.8)	<0.01

[a]Product yield (%) and total conversion of the 2-propanol/*m*-cresol alkylation in two consecutive runs. Reaction conditions: 3 h, 200 °C, 700 psig He. Feed: 2-propanol/*m*-cresol molar ratio 3, total molar concentration 2 M, 500 mg catalyst. All experiments were repeated twice, and the reported values correspond to averages; the errors in these repetitions are indicated in parentheses.

3.5. Characterization of the Zeolites after Reaction. In addition to the differences in adsorption and activity observed on the untreated and functionalized zeolites, there is an important difference in the resistance to morphological deterioration that typically occurs during reaction in the liquid phase at high temperature.[4] First, as shown in Figure 7, no
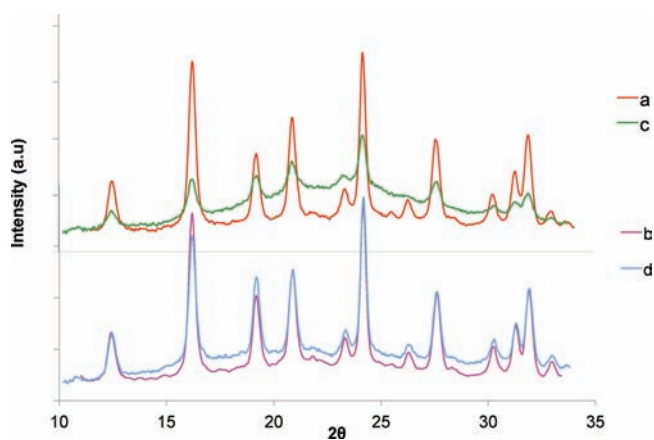

Figure 7. X-ray diffraction of the HY zeolites (Si/Al = 30). Untreated zeolite, before (a) and after reaction (c); OTS-functionalized zeolite, before (b) and after reaction (d). Alkylation reaction conditions same as those in Figure 5 and Table 1. Reaction time: 3 h.

changes in the XRD profiles of the hydrophobic zeolite are seen after reaction, which indicates that the structure of the functionalized sample remains largely undisrupted after exposure to the aqueous environment at 200 °C. By contrast, a dramatic drop in diffraction intensity is observed after reaction on the untreated hydrophilic zeolite, indicating a significant loss of crystallinity. Interestingly, this loss in crystallinity is not accompanied by any shifts in the position of the diffraction peaks, which indicates that the destruction of the untreated zeolite in liquid water is not a selective leaching of cations, which may change the unit cell size, it is rather a drastic collapse of the crystals. As indicated by Ravenelle et al.,[4] this process is different from the better-known dealumination by steaming that occurs at much higher temperatures and in the vapor phase. By contrast, this destruction does not occur on the OTS-functionalized zeolite. This striking difference clearly

shows that the severely deactivating effect of hot liquid water can be minimized by hydrophobic functionalization, which dramatically inhibits the direct interaction and exchange of mass with the bulk liquid water.

The contrasting behavior of the OTS-functionalized zeolite compared to the untreated zeolite was even more clearly evident from the electron microscopy images obtained on the same samples before and after reaction. Both HRTEM (Figure 8) and SEM (Figure 9) demonstrate that the crystalline
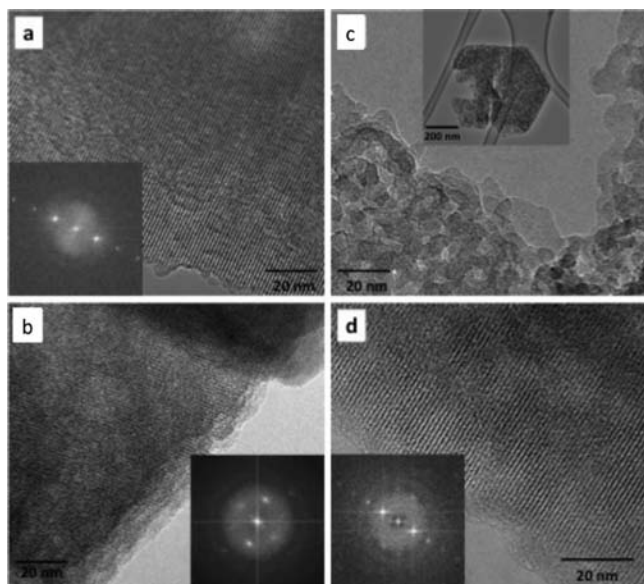

Figure 8. Electron microscopy (HRTEM) of the HY zeolites (Si/Al = 30). Untreated zeolite, before (a) and after reaction (c); OTS-functionalized zeolite, before (b) and after reaction (d). Alkylation reaction conditions same as those in Figure 5 and Table 1. Reaction time: 3 h.

Figure 9. Scanning electron microscopy (SEM). Untreated zeolite, before (a) and after reaction (c); OTS-functionalized zeolite, before (b) and after reaction (d). Alkylation reaction conditions same as those in Figure 5 and Table 1. Reaction time: 3 h.
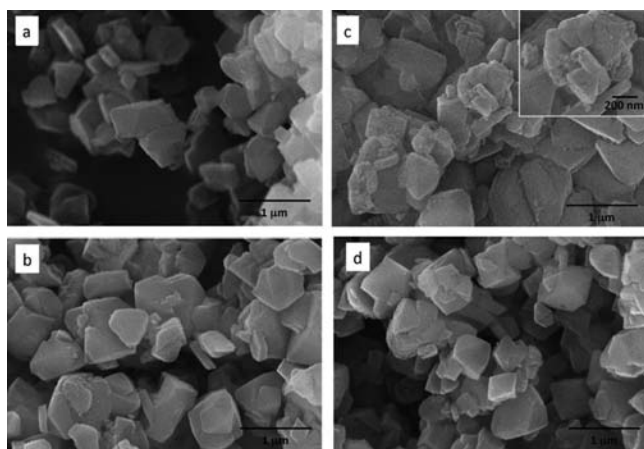
structure of the functionalized zeolite remains unchanged after reaction, while that of the hydrophilic zeolite is greatly affected. The HRTEM of the used OTS-functionalized zeolite (Figure 8d) clearly shows that the ordered patterns of the microporous structure of the zeolite remain practically identical to those of the zeolite before reaction (Figure 8c). By contrast, in the

untreated zeolite (Figure 8b) they disappear after reaction. Similarly, the SEM images indicate that while the external surface of the functionalized zeolite particles does not exhibit a significant change in texture after reaction (see Figure 9c,d), a significantly rougher surface is observed on the untreated zeolite after reaction in the hot liquid water (see Figure 9 b).

In perfect agreement with these observations, the BET surface area and pore size distribution measurements on the four samples give further evidence for the remarkable difference in stability upon exposure to an aggressive liquid environment. As shown in Figure 10, while the adsorption isotherms of the
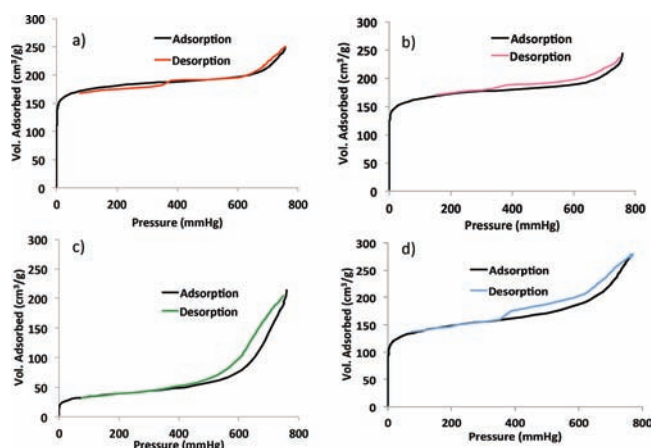

Figure 10. N_2 adsorption/desorption isotherms on the HY zeolites (Si/Al = 30). Untreated zeolite, before (a) and after reaction (c); OTS-functionalized zeolite, before (b) and after reaction (d). Alkylation reaction conditions same as those in Figure 5 and Table 1. Reaction time: 3 h.

untreated sample shows a drastic change after reaction (Figure 10a,b), the change for the OTS-functionalized sample is relatively minor (Figure 10c,d). As summarized in Table 5,

Table 5. Specific Area (S_{BET}) and Pore Volume of the Two HY Zeolites (Untreated and OTS-Functionalized) before and after Reaction[a]

sample	S_{BET}, m²/g	V_{total}, cm³/g	V_{micro}, cm³/g	V_{meso}, cm³/g	S_{micro}, m²/g	S_{meso}, m²/g	V_{meso}/V_{micro}
			Untreated HY				
before reaction	690	0.35	0.27	0.07	660	30	0.26
after reaction	215	0.41	0.01	0.40	35	180	40
			Functionalized HY				
before reaction	640	0.33	0.25	0.08	600	40	0.32
after reaction	530	0.38	0.18	0.20	430	100	1.1

[a]Alkylation reaction conditions: 3 h at 200 °C and 700 psi of He. Feed: 2-propanol/m-cresol, molar ratio 3; total molar concentration 2 M.

the resulting BET surface areas, pore volumes, and micro-/mesopores ratio all reflect this contrasting behavior. Specifically, it should be noted that the surface areas of the functionalized and untreated zeolites are similar, which is in agreement with the conclusion reached above regarding the absence of significant pore plugging due to functionalization. Additionally, the drop in surface area after liquid-phase reaction is only 17%
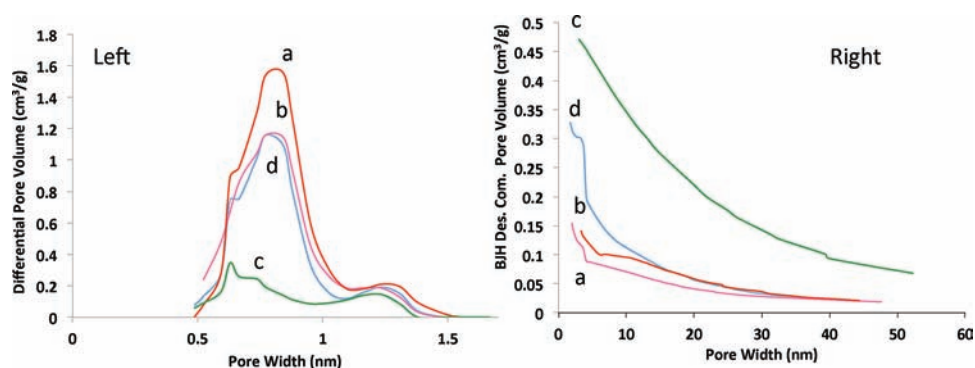
Figure 11. Pore size distribution estimated from the N_2 adsorption/desorption isotherms on the untreated HY zeolite before (a) and after reaction (c) and OTS-functionalized zeolite before (b) and after reaction (d). Left: differential pore volume of the micropores (calculated by the DFT method). Right: desorption cumulative pore volume of the mesopores (calculated by the BJH method).

for the hydrophobic zeolite, but almost 70% for the untreated zeolite.

An analysis of the variation in micro- and mesoporosities after reaction in hot liquid is important to further understand the destruction of the zeolite structure and its prevention by enhancing the hydrophobicity. First, one can see that the microporosity of the hydrophilic zeolite practically disappears when it is exposed to the hot liquid medium. That is, as shown in Table 5, the ratio meso-/microporosity goes from about 0.3 to about 40. It is then no surprise that the catalytic activity of this sample practically vanishes after a few hours in the medium and cannot be restored by drying. As illustrated in Figure 11a, the micropore size distributions obtained by DFT analysis of the N_2 physisorption data show similar behavior. That is, no significant differences in pore distribution between the functionalized and untreated samples before reaction, but a dramatic degradation on the hydrophilic zeolite after reaction. Interestingly, as shown in Figure 11b, this degradation of micropores is paralleled by an increase in mesoporosity. The structural conversion of microporosity into mesoporosity is an indication that, as mentioned above, the zeolite degradation process of the untreated zeolite can be described as a collapse of the crystallites, which give rise to internal mesopores. It is important to point out the critical differences in the extent of zeolite degradation occurring in the presence of hot liquid water compared to steam at comparable temperatures. That is, while steaming at 200 °C would cause little if any change in crystallinity,[45] heating in liquid water at the same temperature caused almost a total destruction of the crystallites. Therefore, one may conclude that the hydrophobization of the external surface of the zeolite prevents the contact of the crystallites with liquid water, which readily destroys the hydrophilic zeolite via hydrolysis accelerated by solvation and rapid mobility of the ions into the liquid phase.

3.6. Alkylation Reaction in a Real Bio-oil Sample. To test these hydrophobized zeolites in a real bio-oil, we prepared a mixture of 2-propanol and *m*-cresol in pyrolysis oil dissolved in water/decalin emulsion. While the alkylation conversion was lower than what we typically observed in clean mixtures, we did obtain alkylation products, not only from *m*-cresol, but also from the phenolics present in bio-oil, demonstrating the applicability of this reaction strategy to real biomass conversion. For this test, bio oil obtained from fast pyrolysis of switchgrass was pretreated in bubbling H_2 in the presence of Ru/TiO$_2$ (reduced at 400 °C). The resulting hydrogenated bio-oil was added to the *m*-cresol and 2-propanol mixture and fed into the

batch reactor in a previously prepared water/decalin an emulsion stabilized by OTS-functionalized HY zeolite. The reaction conditions were 200 °C, 700 psig He, 0.5 M *m*-cresol, and 2-propanol/*m*-cresol molar ratio 3. The GC-FID analysis of the product showed about 1% monoalkylated products and 1.6% dialkylated products. The *m*-cresol alkylation activity is lower in the bio-oil than with pure feed due to the numerous side reactions that occur in presence of the bio-oil. However, the GC analysis indicated that many of the other bio-oil compounds (phenol, benzofuran, acetic acid, and acetone) were converted into larger alkyl aromatics due to alkylation catalyzed by the hydrophobic zeolite. These are beneficial reactions in the production of biofuels because they lead to longer chain hydrocarbons and more stable bio-oils, incorporating smaller oxygenates to the fuel range, which otherwise would end up as water-soluble compounds or as light gases when hydrotreated.

4. CONCLUSIONS

In summary, by functionalizing the surface of the HY zeolite with hydrophobic octadecyltrichlorosilane, we have tailored it for use in hot aqueous media, as is necessary for the refining of biomass pyrolysis oil. This modification, which stabilizes the zeolite against losses of crystallinity, greatly enhances the catalytic activity, regenerability, and reusability of solid catalysts in biphasic emulsion systems. An important concept presented here is that hydrophobization of the external surface of a zeolite protects it against destruction of its structure while keeping its active sites (in this case H$^+$) inside, practically unaltered, when used in reactions involving hot liquid water.

At moderate temperatures (e.g., 100−200 °C) water vapor does not cause any significant degradation of the zeolite structure, but liquid water does. Therefore, the role of the hydrophobic barrier is to prevent the contact of the zeolite with the liquid water, preventing the extensive hydrolysis accelerated by solvation and rapid ion mobility, which readily occurs with a conventional hydrophilic zeolite.

We propose that these hydrophobic protective layers could be applied to other catalytic species, such as metal clusters, basic sites, sulfonic groups, and other active species anchored inside the channels of a porous material to be used in aqueous systems at temperatures above 100 °C.

■ AUTHOR INFORMATION

Corresponding Author
resasco@ou.edu

Author Contributions

#P.A.Z. and J.F. contributed equally to this work.

Notes

The authors declare no competing financial interest.

REFERENCES

(1) Huber, G. W.; Iborra, S.; Corma, A. *Chem. Rev.* **2006**, *106*, 4044–4098.

(2) Luo, C.; Wang, S. A.; Liu, H. C. *Angew. Chem., Int. Ed.* **2007**, *46*, 7636–7639.

(3) Román-Leshkov, Y.; Chheda, J. N.; Dumesic, J. A. *Science* **2006**, *312*, 1933–1937.

(4) Ravenelle, R. M.; Schüäler, F.; D'Amico, A.; Danilina, N.; van Bokhoven, J. A.; Lercher, J. A.; Jones, C. W.; Sievers, C. *J. Phys. Chem. C* **2010**, *114*, 19582–19595.

(5) Cejka, J.; Corma, A.; Zones, S. I. *Zeolites and catalysis: Synthesis, reactions and applications*; Wiley: New York, 2010.

(6) Okuhara, T. *Chem. Rev.* **2002**, *102*, 3641–3666.

(7) Nishimiya, K.; Tsutsumi, K. *Thermochim. Acta* **1989**, *143*, 299–309.

(8) Corma, A.; Domine, M. E.; Valencia, S. *J. Catal.* **2003**, *215*, 294–304.

(9) Corma, A.; Nemeth, L. T.; Renz, M.; Valencia, S. *Nature* **2001**, *412*, 423–425.

(10) Moliner, M.; Román-Leshkov, Y.; Davis, M. E. *Proc. Natl. Acad. Sci. U.S.A.* **2010**, *107*, 6164–6168.

(11) Nur, H.; Ikeda, S.; Ohtani, B. *J. Catal.* **2001**, *204*, 402–408.

(12) Meininghaus, C. K. W.; Prins, R. *Microporous Mesoporous Mater.* **2000**, *35–36*, 349–365.

(13) Zhao, X. S.; Lu, G. Q. *J. Phys. Chem. B* **1998**, *102*, 1556–1561.

(14) Inagaki, S.; Ima, H.; Tsujiuchi, S.; Yakushiji, H.; Yokoi, T.; Tatsumi, T. *Microporous Mesoporous Mater.* **2011**, *142*, 354–362.

(15) Shen, M.; Resasco, D. E. *Langmuir* **2009**, *25*, 10843–10851.

(16) Faria, J.; Ruiz, M. P.; Resasco, D. E. *Adv. Synth. Catal.* **2010**, *352*, 2359–2364.

(17) Ruiz, M. P.; Faria, J.; Shen, M.; Drexler, S.; Prasomsri, T.; Resasco, D. E. *ChemSusChem* **2011**, *4*, 964–974.

(18) Zapata, P. A.; Faria, J.; Ruiz, M. P.; Resasco, D. E. *Top. Catal.* **2012**, *55*, 38–52.

(19) Binks, B. P.; Lumsdon, S. O. *Langmuir* **2000**, *16*, 2539–2547.

(20) Crossley, S.; Faria, J.; Shen, M.; Resasco, D. E. *Science* **2010**, *327*, 68–72.

(21) Huber, G. W.; Chheda, J. N.; Barrett, C. J.; Dumesic, J. A. *Science* **2005**, *308*, 1446–1450.

(22) Román-Leshkov, Y.; Barrett, C. J.; Liu, Z. Y.; Dumesic, J. A. *Nature* **2007**, *447*, 982–985.

(23) Singh, R.; Dutta, P. K. *Microporous Mesoporous Mater.* **1999**, *32*, 29–35.

(24) Sing, K. S.W.; Williams, R. T. *Adsorption Sci. Technol.* **2004**, *22*, 773–782.

(25) Mirji, S. A. *Surf. Interface Anal.* **2006**, *38*, 158–165.

(26) Jeon, N. L.; Finnie, K.; Branshaw, K.; Nuzzo, R. G. *Langmuir* **1997**, *13*, 3382–3391.

(27) Hoffmann, H.; Mayer, U.; Krischanitz, A. *Langmuir* **1997**, *11*, 1304–1312.

(28) Mirji, S. A.; Halligudi, S. B.; Sawant, D. P.; Jacob, N. E.; Patil, K. R.; Gaikwad, A. B.; Pradhan, S. D. *Appl. Surf. Sci.* **2006**, *252*, 4097–4103.

(29) Flinn, D. H.; Guzonas, D. A.; Yoon, R.-H. *Colloids Surf. A: Physicochem. Eng. Aspects* **1994**, *87*, 163–176.

(30) Tripp, C. P.; Hair, M. L. *Langmuir* **1994**, *11*, 1215–1219.

(31) Makarova, M. A.; Ojo, A. F.; Karim, K.; Hunger, M.; Dwyer, J. *J. Phys. Chem.* **1994**, *98*, 3619–3623.

(32) van Santen, R. A. *Stud. Surf. Sci. Catal.* **1994**, *85*, 273–294.

(33) Jacobs, W. P. J. H.; Jobic, H.; van Wolput, J. H. M. C.; van Santen, R. A. *Zeolites* **1992**, *12*, 315–319.

(34) Koranyi, T. I.; Moreau, F.; Rozanov, V. V.; Rozanova, E. A. *J. Mol. Struct.* **1997**, *410*, 103–110.

(35) Kazansky, V. B.; Serykh, A. I.; Semmer-Herdelan, V.; Frasissard, J. *Phys. Chem. Phys. Chem.* **2003**, *5*, 966–969.

(36) Northcott, K. A.; Bacus, J.; Taya, N.; Komatsu, Y.; Perera, J. M.; Stevens, G. W. *J. Hazardous Mater.* **2010**, *183*, 434–440.

(37) Ouki, S. K.; Kavannagh, M. *Waste Manag. Res.* **1997**, *15*, 383–394.

(38) Collignon, F.; Poncelet, G. *J. Catal.* **2001**, *202*, 68–77.

(39) Kawai, T.; Tsutsumi, K. *Colloid Polym. Sci.* **1998**, *276*, 992–998.

(40) Mapes, J. E.; Eischens, R. P. *J. Phys. Chem.* **1954**, *58*, 1059–1062.

(41) Farneth, W. E.; Gorte, R. J. *Chem. Rev.* **1995**, *95*, 615–635.

(42) Viswanathan, B.; Jacob, B. *Catal. Rev. Sci. Eng.* **2005**, *47*, 1–82.

(43) Vinu, A.; Kumar, G. S.; Ariga, K.; Murugesan, V. *J. Mol. Catal. A: Chem.* **2005**, *235*, 57–66.

(44) Madon, R. J.; Iglesia, E. *J. Mol. Catal. A: Chem.* **2000**, *163*, 189–204.

(45) McDaniel, C. V.; Maher, P. K. *Molecular Sieves*; Society of the Chemical Industry: London, 1968; pp 186–195.